World Conference on Timber Engineering Oslo 2023

FIBRE-OPTIC MEASUREMENTS FOR MONITORING ADHESIVELY BONDED TIMBER-CONCRETE COMPOSITE BEAMS

Jens Frohnmüller[1], Werner Seim[2], Ann-Charlotte Spangenberg[3]

ABSTRACT: The technology of fibre-optic sensors (FOS) enables the continuous measurement of strains along the fibre axis. This offers the possibility of studying and monitoring the behaviour of the component to which the fibre is connected at any given point. In this paper, the FOS measurement technique is applied aiming to develop a monitoring tool for checking the integrity of the adhesively bonded joint between timber and concrete. Accordingly, tests with adhesively bonded timber-concrete composite beams, which have been loaded up to ultimate failure, are conducted. The measurement results are presented and checked for plausibility with the aid of an finite element model. Subsequently, a calculation model is presented with which the shear stresses in the adhesive joint can be derived directly from the strain measurements. As a result, it can be stated that it has been possible to monitor the integrity of the bonded joint and derive shear stresses directly from the measurement, however, more research is necessary to get an even better understanding of how to analyse and post-process the measurement data.

KEYWORDS: Fibre-optical measurement, Monitoring, Adhesives, Timber-Concrete Composites, Quality control

1 INTRODUCTION

1.1 FIBRE-OPTIC SENSORS – TYPICAL AREAS OF APPLICATION

The technology of fibre-optic sensors (FOS) allows the measurement of strains continuously along the length of the sensor. This offers new and promising possibilities for the testing of structural elements in the laboratory, and especially for the on-site monitoring of load-bearing elements if possible damage can be identified.

The FOS were used, for example, by Schmidt-Thrö et al. [1] and Lemcherreq et al. [2] to investigate the basic behaviour of the fibres in the case of the bond between reinforcement steel and concrete. The optic fibre was glued onto the steel-rod in this case.

A quite extensive report on FOS for use in structural bondlines was reported by Könke et al. [3], who also investigated the use of the technology as a monitoring tool for adhesively bonded timber-concrete composite (ATCC) beams. Könke et al. hereby observed, for example, that cracks in the concrete plate could be detected. Similar observations were documented by Spangenberg [4], who identified knot-holes and air bubbles of the adhesive, which had been used to apply the fibre onto an ATCC specimen, as peak values in the measurement.

In the field of timber structures, a comparable measurement method, so-called Fibre Bragg Grating (FBG), was used by Claus et al. [5] to investigate the force distribution in self-tapping screws in timber. New effects regarding the load distribution in the interface between screw and timber could be seen and the effective embedding length of the screws was considered in more detail, comparing it to Volkersen's theory.

1.2 AIM AND APPROACH

The aim is to investigate how FOS can be used for the monitoring of structural elements, focusing on the adhesive bondline. Firstly, the materials and methods are presented. The results of the measurements for two different test series are then presented. In both cases, the strains in the adhesive joint are measured, and in one case, additionally the strains at the bottom edge of the timber (see exemplarily one of the specimens from test series ATCC-A in Figure 1).

In a next step, the experimental measurement data are validated and checked for plausibility by means of a finite element (FE) model. A calculation model is then presented, with which the shear stresses in the bondline can be determined directly from the measurement.

2 MATERIALS & METHODS

2.1 EXPERIMENTAL PROGRAMME AND TEST SET-UP

The experimental programme covers two types of specimens. The cross-section and the location of the FOS are depicted in Figure 1 (ATCC-A) and Figure 2 (ATCC-B).

[1] Jens Frohnmüller, University of Kassel, Timber Structures and Building Rehabilitation, Germany, jens.frohnmueller@uni-kassel.de
[2] Werner Seim, University of Kassel, Timber Structures and Building Rehabilitation, Germany.
[3] Ann-Charlotte Spangenberg, DB Netz AG, Kassel, Germany.

https://doi.org/10.52202/069179-0103

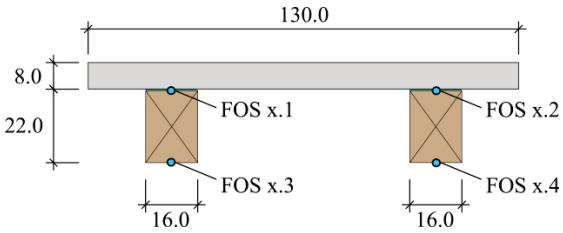

Figure 1: *Geometry and location of FOS for specimens of series ATCC-A*

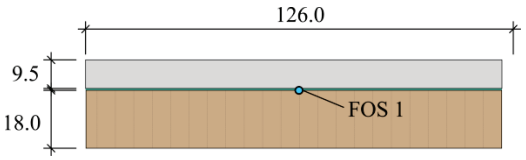

Figure 2: *Geometry and location of the FOS for specimens of series ATCC-B*

Regarding the specimens of the series ATCC-A, the FOS have been placed in the bondline (FOS x.1 and FOS x.2) and on the bottom edge of the timber beam (FOS x.3 and FOS x.4) continuously along its length. Concerning the specimen ATCC-B, one FOS has been installed directly in the bondline. The relevant parameters and decisive differences between the two types are summarised in Table 1.

Table 1: *Experimental programme*

Parameter	Type	
	ATCC-A	ATCC-B
Number of specimens	3	1
Span	6.00 m	7.68 m
Bond arrangement	Continuous (full length)	Discontinuous (strips)
Adhesive	Low viscous epoxy (2EP)	Polymer mortar (2EP)
Timber geometry	Beam	Plate
Timber quality	GL24h	GL28c
Concrete quality	C45/55	C40/50
Number of FOS per specimen	4	1

The bottom surface of the prefabricated concrete parts of ATCC-A has not been further processed after removing the formwork. The bottom surface of the concrete parts of ATCC-B has been sandblasted.

The ATCC specimens were tested in a 4-point bending configuration similar to that by Frohnmüller et al. [6]. The force was measured with a load cell, and the mid-span deflections and the relative displacement between timber and concrete with displacement transducers. The measurement was performed at a sampling rate of 2 Hz. The distance between each measurement point on the sensor length was chosen to be 1.3 mm. This led to approximately 12,000 data points (ATCC-A) and 14,500 data points (ATCC-B) along the span per second.

The strains ε_x could be converted, considering Young's Modulus E_x, into stresses σ_x using Equation 1.

$$\sigma_x = \varepsilon_x \cdot E_x \quad (1)$$

2.2 SPECIMEN MANUFACTURING

The FOS were installed by cutting a small groove at a depth of 5 mm into the timber part, laying the sensors into the groove and filling it up with a low viscosity epoxy adhesive. During hardening, the adhesive was sucked into the timber part at several points due to knot-holes or small cracks. Small air bubbles appeared in these areas, and were then pierced before more adhesive was applied.

The manufacturing process of gluing timber and concrete was different for the two test series.

2.2.1 ATCC-A

The concrete plate was turned on its back and spacers with a thickness of 2 mm were placed on the slab. The timber beams were then placed on top. They had been drilled previously at regular intervals with holes through the height of the beam. After a circumferential sealing of the joint, the adhesive was injected through the holes which were then successively closed utilising beech wood dowels. The bond width was reduced to 75 % of the original width for specimen -02 and to 50 % for specimen -03 for each beam.

2.2.2 ATCC-B

The polymer mortar for the second type was applied on the timber part with a mortar sledge, into which a toothed spatula had been installed. The prefabricated concrete plate was then placed on top of the timber plate. No turning of the concrete plate was necessary.

3 TEST RESULTS

3.1 ATCC-A

The global failure occurred in all three cases as a bending failure in the timber beam at a load level of $F_{u,exp}$ = 109 kN (ATCC-A-01), $F_{u,exp}$ = 153 kN (ATCC-A-02) and $F_{u,exp}$ = 165 kN (ATCC-A-03), whereby $F_{u,exp}$ is the load applied by the actuator. Additionally, the self-weight F_G = 11 kN of the steel structure to transfer the load must be added. The specimen ATCC-A-01 showed the peculiarity that a local bending failure occurred in the outer lamella of one beam of the timber at a load level of $F_{u,exp}$ = 93 kN. Further loading was possible up to global bending failure. The adhesive joint remained intact, with a negligible relative displacement between the timber and the concrete for all specimens.

The results of the FOS measurements along the bond length of all three specimens are shown in Figure 3. The measurement results are all presented for the same load step F_{exp} = 75 kN for reasons of comparability.

https://doi.org/10.52202/069179-0103

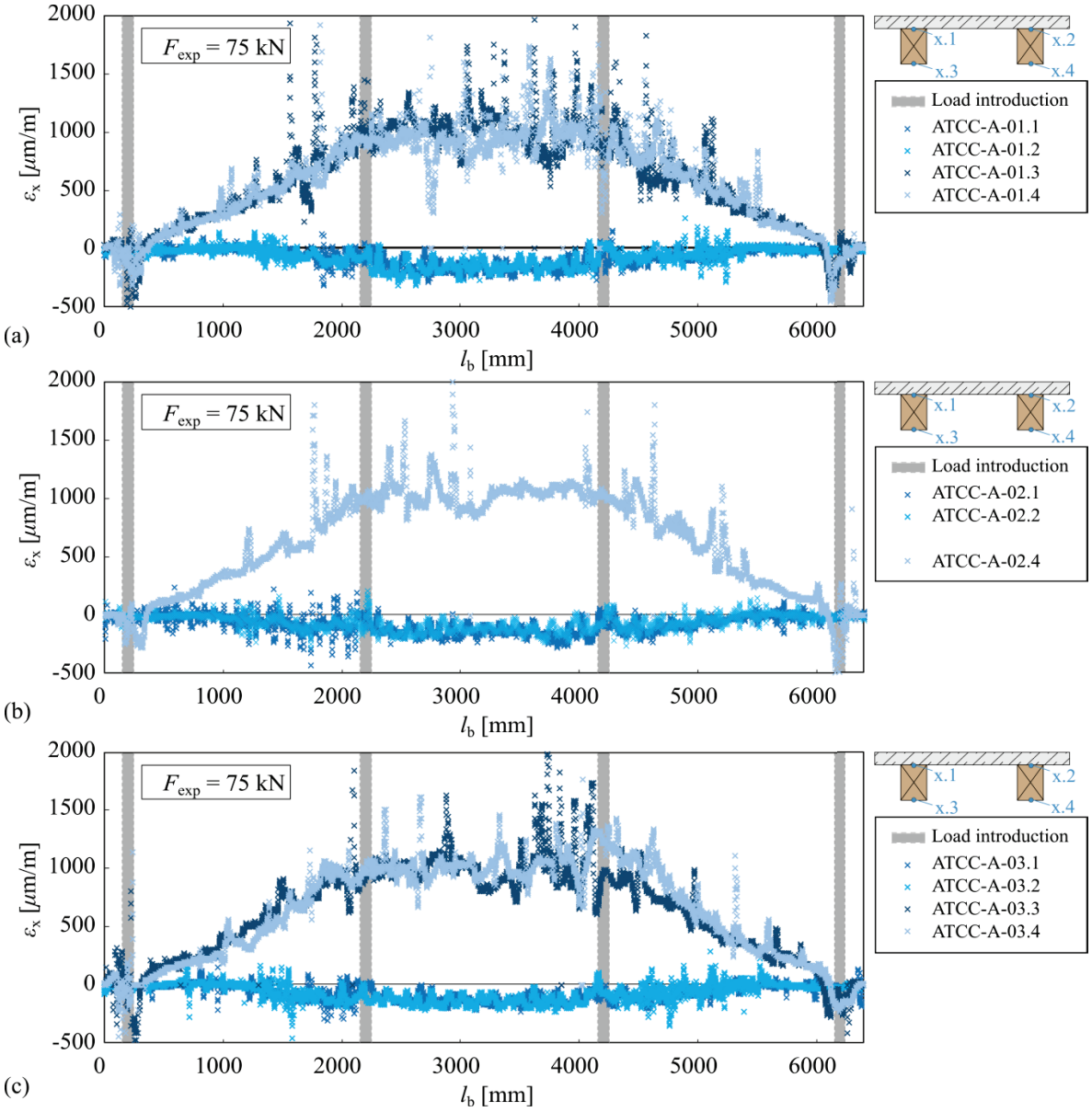

Figure 3: *Results of the fibre-optic measurements – ATCC-A-01 to ATCC-A-03. Strains ε_x along the bond length for the load step F_{exp} = 75 kN (a) ATCC-A-01, (b)B ATCC-A-02 and (c) ATCC-A-03*

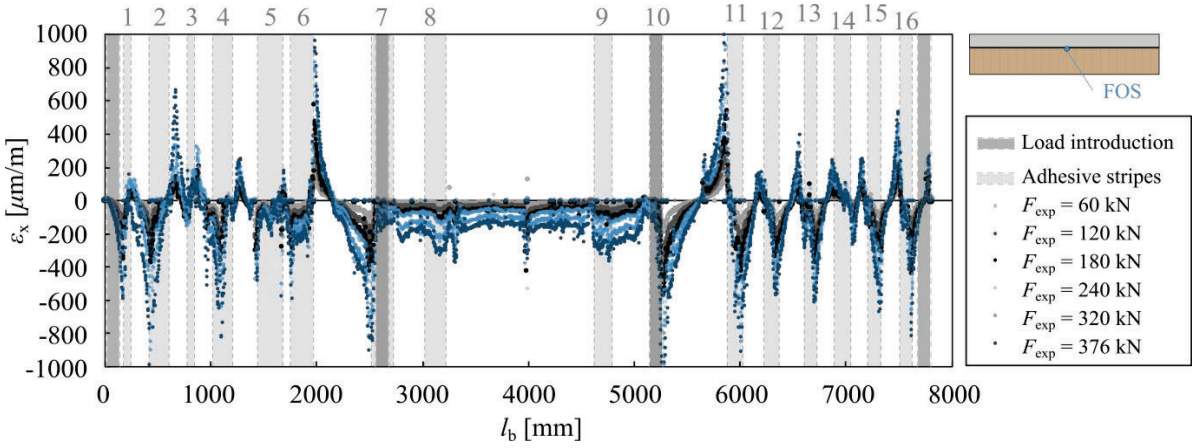

Figure 4: *Results of the fibre-optic measurements – ATCC-B. Strains ε_x along the bond length for the six load steps (The scale in the range of -1000 μm/m to +1000 μm/m is depicted; individual strain values are larger)*

https://doi.org/10.52202/069179-0103

The force from the actuator is F_{exp}, since the measurement was zeroed before the start of the FOS measurement. The steel structure for the load transfer was installed before the start and the zeroing of the measurement. No measurement data is available for the fibre 2.3 in Figure 3b due to a breakage during the installation of the fibre into the testing field.

The large peaks in the measurement (Figure 3) indicate local irregularities in the timber part, such as knot-holes or air bubbles in the adhesive used to glue the fibre into the groove. Smaller deviations are associated with cracks in the concrete, as observed by Könke et al. [3], or knot-holes in the timber, which were in close proximity to the fibre (approximately 10 to 50 mm).

A quasi linear-elastic load-displacement behaviour was observed during all three tests of the series ATCC-A. The same applies to the majority of the FOS measurement data which can be seen in Figure 5, where the normalized strains $\varepsilon_x/\varepsilon_{x,max} < 1.0$ of two different load steps are depicted. The load step $F_{u,exp} = 93$ kN complies with the load step immediately before the failure. However, an irregular behaviour of the strains becomes visible in certain areas.

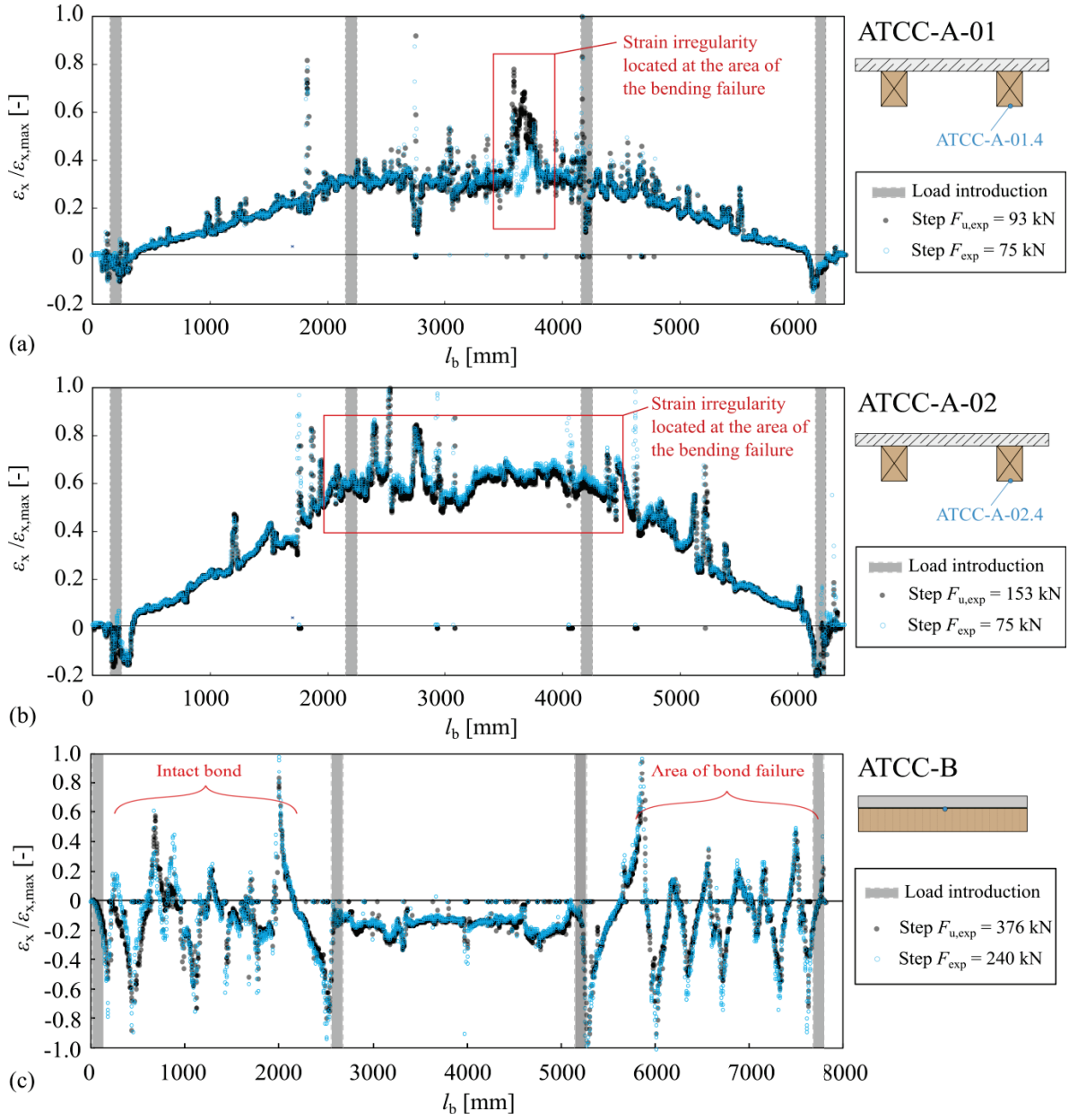

Figure 5: *Comparison of normalised strains $\varepsilon_x/\varepsilon_{x,max}$ for two load steps and (a) ATCC-A-01 (b) ATCC-A-02 and (c) ATCC-B*

https://doi.org/10.52202/069179-0103

The change of the strains of ATCC-A-01.4 happened comparatively suddenly and was concentrated locally on a certain section (Figure 5a). The sensor ATCC-A-03.3 showed a comparable behaviour.

The other sensors, ATCC-A-01.3, ATCC-A-02.4 and ATCC-A-03.4, showed a different behaviour, because the change was not concentrated but distributed mostly in the inner third of the span, where the largest bending stress occurred (Figure 5b). The irregularity in the inner third of the span happened in contrast to the irregularity which was concentrated locally, continuously over time.

3.2 ATCC-B

The failure of the composite beam occurred as expected as a combined bond failure in the timber and the concrete at a load level of $F_{u,exp}$ = 376 kN. The bond failure took place simultaneously at the strips no. 11-16 in the area of l_b = 5.0 …8.0 m and has been characterised purely by a mixed substrate failure in the timber and the concrete and no adhesion or cohesion failure could be documented. Further details of the full-scale test can be found in Frohnmüller et al. [6]. The strains measured are depicted for several load steps in Figure 4. The largest strain gradient in terms of magnitude occurred in the adhesive strip no. 11. The strains generally increased to the same extent as the load steps. Regarding the load-displacement behaviour, a linear elastic behaviour was present. This could also be confirmed for the strains based on Figure 5c, where no explicit irregularities were detected.

4 VALIDATION OF THE MEASUREMENT

4.1 FINITE ELEMENT MODEL

A validation of the strain measurement is possible by means of an FE model. The latter is implemented using the software package ABAQUS and is based on two-dimensional shell elements with a mesh size of a_E = 5.0 mm, which corresponds to about 60 FEs over the height of the component for the test series ATCC-A and 56 for the test series ATCC-B. The model consists of CPS4R elements with four nodes and one integration point in the centre of the element (reduced integration). The path where the strains are evaluated was chosen similar to the location of the FOS. The FE model is depicted exemplarily for one specimen of the type ATCC-A in Figure 6.

Both bending and bond failure occurred in a brittle manner and a linear-elastic load-displacement behaviour could be seen in the tests, therefore, linear-elastic material properties were assigned. Local axes were defined to account for the anisotropy of the timber. This orthotropic material behaviour of the timber is modelled in ABAQUS using parameters as documented in Table 2.

Table 2: *Stiffness properties of timber*

Quality	E_x [N/mm²]	E_z [N/mm²]	ν_{xz} [-]	G_{xz} [N/mm²]
GL24	11.500	510	0.45	650
GL28	12.500	510	0.45	710

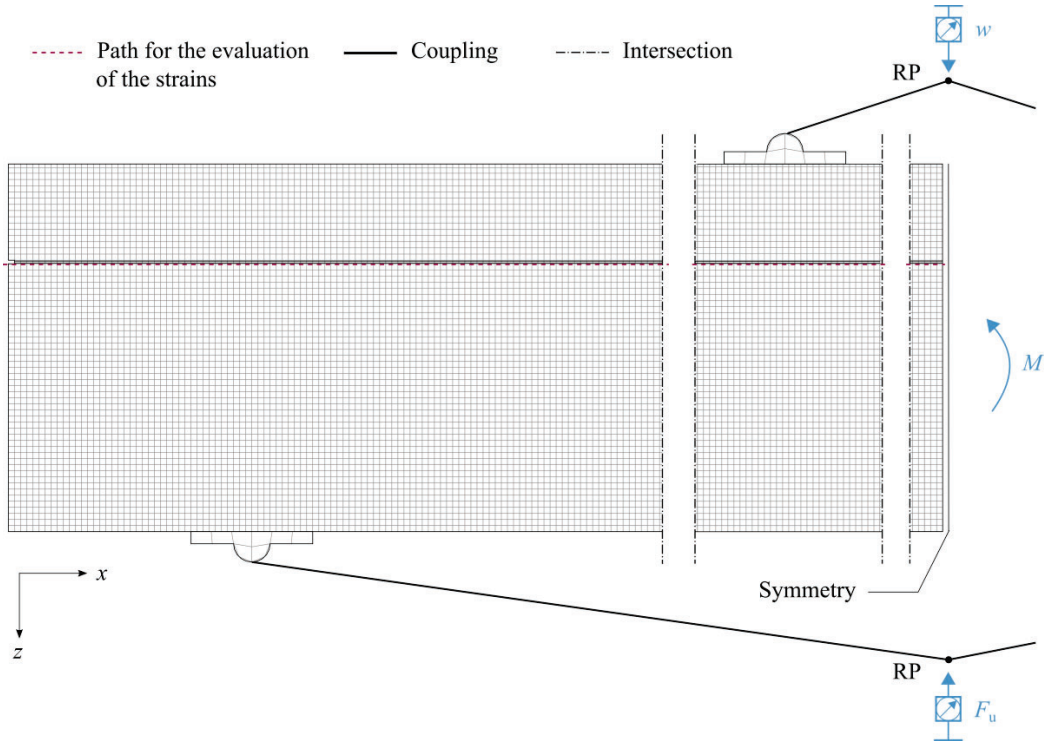

Figure 6: *Finite Element (FE) Model*

https://doi.org/10.52202/069179-0103

The isotropic material properties of concrete and adhesive are summarised in Table 3.

Table 3: *Stiffness properties of concrete and adhesive*

Material	E_x [N/mm²]	ν_{xz} [-]	G_{xz} [N/mm²]
Concrete C40/50	33.000	0.20	13.750
Concrete C45/55	34.500	0.20	14.375
2EP, low viscosity	2.500	0.40	893
Polymer mortar	25.000	0.30	10.500

4.2 COMPARISON OF MEASUREMENT AND FE MODEL

A comparison of the strains between the measurement and the FE model for type ATCC-A is depicted in Figure 7a and Figure 7b exemplarily for both beams of the specimen ATCC-A-03. The results of the FOS are depicted for the ultimate load step $F_{u,exp}$ = 165 kN.

Regarding ATCC-A, the general shape of the measurement data stands in good accordance with the results from the FE calculation. The maximum strains, however, are, in some parts, significantly higher than assumed by the calculation. Some of these peak values may be attributed to air bubbles in the adhesive with

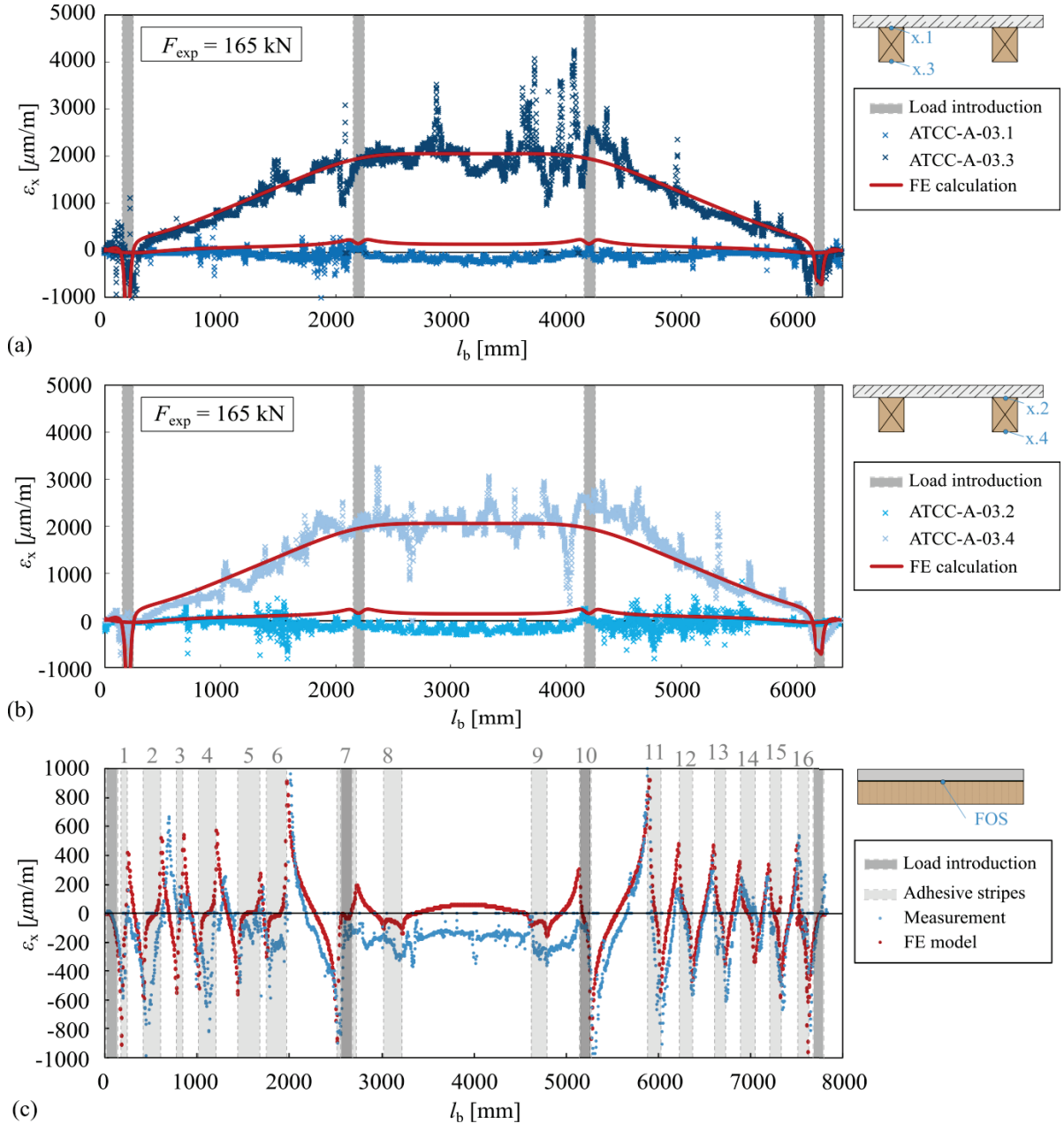

Figure 7: *Strains ε_x – comparison of measurement and FE model for ATCC-A-03*

https://doi.org/10.52202/069179-0103

which the fibre has been glued into the groove or knot-holes in the timber, as noted by Spangenberg [4]. Nevertheless, some strains clearly exceed the calculation.

A comparison of the strains between the measurement and the FE model for the composite of specimen ATCC-B is depicted in Figure 7c. A good accordance in the area of l_b = 5.5 … 8.0 m, where the bond failure occurred, can be seen both in the area of the adhesive strips and between them. It becomes evident that the bond at every strip is active, because otherwise there would no strain gradient.

Certain deviations concerning the beginning and the end of the individual adhesive strip can be seen in the area of l_b = 0 … 2.5 m and, therefore, also in the maximum and minimum values.

It should be noted that the general shape of the data curves in the area between the strips at l_b = 2.5 … 5.5 m are comparable, however, the measurement shows a timber component which is fully under compression, while the FE model indicates that the fibre is more or less located around the neutral axis of the composite beam.

5 SHEAR STRESSES

5.1 DERIVATION FROM MEASUREMENT DATA – PROCEDURE

Regarding the strains measured with FOS, the shear stresses τ_b in the bondline can be calculated directly from the measurement data if the strains have been measured both in the bondline and on the outer edge of the timber beam, resulting in two measurement points per timber beam section, as is the case for test series ATCC-A. The geometric relationships and the step-by-step procedure are shown in Figure 8.

In a first step, the strains measured are converted into stresses using Equation 1. The strains ε_o and ε_u have been averaged for 7 data points, which complies to a length of about 1 cm. The resulting forces in the timber cross-section are then determined by assuming a linear stress distribution over the height of the timber.

$$F_t = \frac{(\sigma_o + \sigma_u)}{2} \cdot A_t \tag{2}$$

The section area A_t is determined considering the height h_t and the width b_t of the timber beam.

$$A_t = h_t \cdot b_t \tag{3}$$

The determination of the force at the right edge of the cut ($F_t + \Delta F_t$) is done in the same way with the stresses at the next measuring point ($\sigma_o + \Delta\sigma_o$) and ($\sigma_u + \Delta\sigma_u$).

$$(F_t + \Delta F_t) = \frac{((\sigma_o + \Delta\sigma_o) + (\sigma_u + \Delta\sigma_u))}{2} \cdot A_t \tag{4}$$

Using the condition of equilibrium of horizontal forces $\sum H = 0$, the shear force in the joint T_b can be determined as:

$$T_b = (F_t + \Delta F_t) - F_t = \Delta F_t \tag{5}$$

The shear stress $\bar{\tau}_b$ derived from the strain can then be calculated by relating T_b to the effective bond area of the surface $A_{\Delta l}$ considered.

When the whole beam width is bonded, the width of the glued joint b_b is equal to the width of the timber beam b_t.

$$\bar{\tau}_b = \frac{T_b}{A_b} \tag{6}$$

with:

$$A_b = b_b \cdot \Delta l \tag{7}$$

The parameter Δl corresponds to the distance between two individual measuring points along the fibre.

The width, the height and the Young's modulus of each timber beam are inserted for the geometrical parameters in Equation 8: b_t = 160 mm, h_t = 220 mm and E_t = 11.500 N/mm². The bond width b_b varies depending on the specimen. For ATCC-A-01, the full width b_b = 160 mm, for ATCC-A-02 the reduced width b_b = 120 mm and for ATCC-A-03 only half of the width b_b = 80 mm is inserted. The length Δl is chosen as Δl = 0.10 m.

5.2 SPECIMENS ATCC-A

The results $\bar{\tau}_b$ of the calculation from section 5.1 are shown exemplarily for the beam 02 of specimen ATCC-A-03 in Figure 9a. The shear stresses $\bar{\tau}_b$ are compared to the shear stresses from the FE calculation. It can be seen that the values of $\bar{\tau}_b$ oscillate around the value of the FE calculation and the maximum and the minimum values differ significantly. A similar behaviour can be

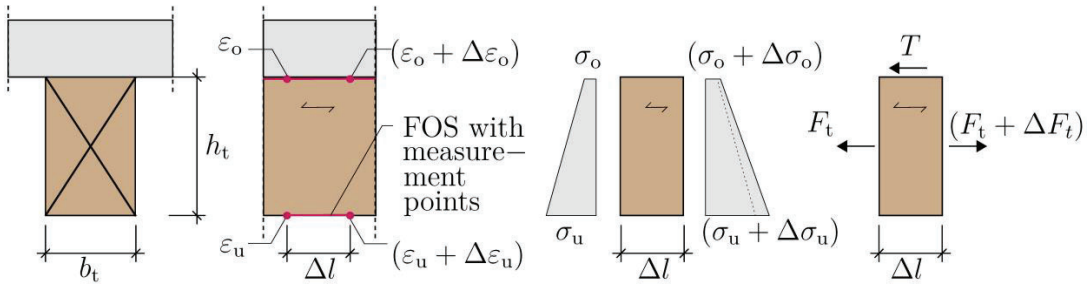

Figure 8: *Model for the derivation of shear stresses*

https://doi.org/10.52202/069179-0103

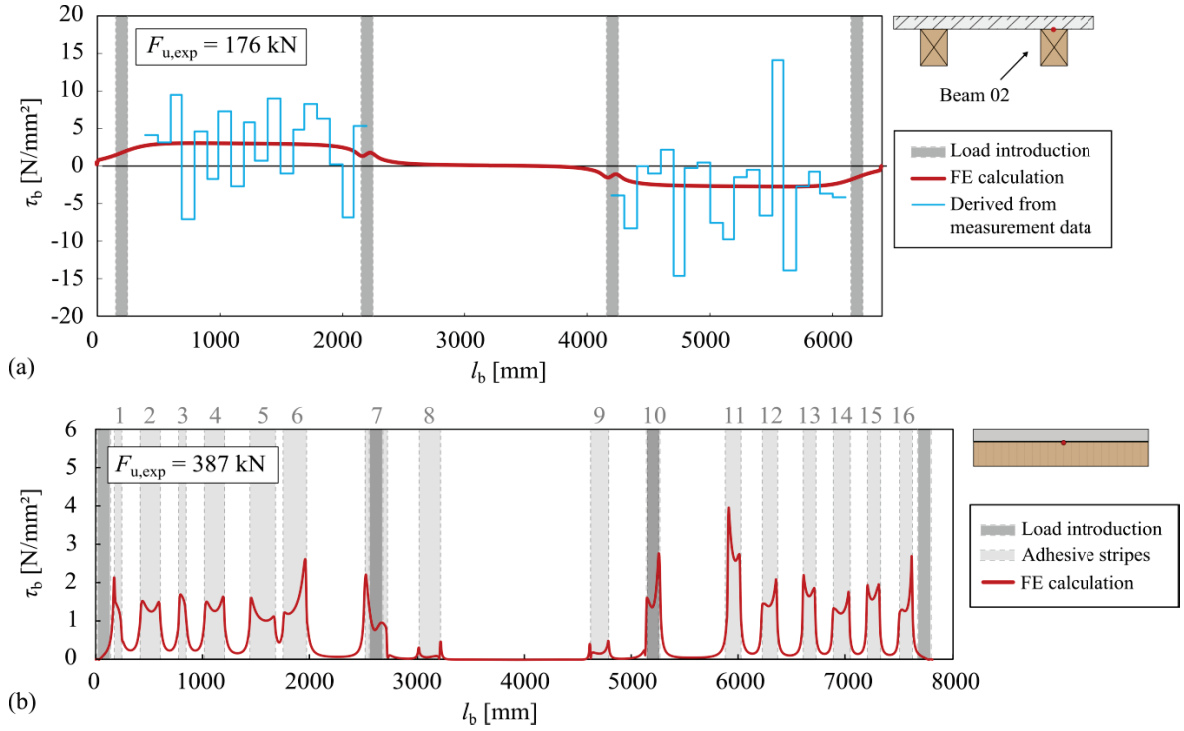

Figure 9: *(a) ATCC-A-03, beam 02: Shear stresses from FE calculation compared to shear stresses derived from measurement data for Δl = 0.10 m, beam 02*
(b) ATCC-B: Shear stresses from the FE calculation

observed for the specimens ATCC-A-01 and ATCC-A-02. At this point, it is important to point out again that these shear stresses are not ultimate shear stresses, since a bending failure in the timber has occurred in the tests and not a bond failure.

5.3 SPECIMEN ATCC-B

Only the shear stresses from the FE calculation for the specimen ATCC-B are shown in Figure 9b, with the maximum shear stress of $\tau_{b,max}$ = 4.0 N/mm² in strip 11. The procedure from section 5.1 cannot be applied there because the derivation of $\bar{\tau}_b$ requires two sensors for each timber beam.

6 CONCLUSIONS & OUTLOOK

The topic of monitoring ATCC components can be subdivided into the question of the control of the bond and the prediction of failure.

In this study, a successful adhesion could be observed by comparing the experimentally determined strains from the measurement with the values from an FE calculation. This applies both for the strains in the actual bondline, since a missing bond would be recognisable from the strain gradient, and the strains in the tension zone, which would have to be significantly greater in the case of a missing bond due to the missing composite action.
The shear transfer could further be visualised for a discontinuous bond arrangement, as is the case with the specimen ATCC-B, by means of a large strain gradient.

Regarding the three specimens from the type ATCC-A, a successful adhesion could be shown based on a calculation model, with which shear stresses have been derived directly from the measurement data. This data, however, is influenced strongly by local irregularities, such as cracks and knot-holes, which lead to a rather unsteady strain curve influenced by peaks and high strain gradients in small increments. Although the shear stresses are basically in a reasonable range, it becomes clear that this procedure is not yet fully matured and that further research is necessary. The aim should be to find either a method to determine a more constant and less unsteady strain measurement or a more robust calculation method for direct shear stress derivation. Approaches to the former can be found, for example, in Galkovski et al. [8] who place a significant emphasis on post-processing of the measurement data.

Regarding the possible prediction of a failure, the strains at the failure load were compared with those from load levels that were more distant from failure. On the basis of three specimens, it could be observed that strains behaved irregularly in some sections. Sudden changes could then indicate an imminent failure. Regarding the other two specimens, no irregular development of the strains could be observed. Whether this different behaviour is due to the fact that the corresponding sensor had not been located at the point of failure or if the irregular strain behaviour just coincided with the failure areas requires further research.
Finally, it can be stated that the FOS technology is a significant improvement compared to strain gauges, because the strips are measured continuously and not only locally, hence, a better understanding of the load transfer in the elements can be achieved.

https://doi.org/10.52202/069179-0103

ACKNOWLEDGEMENTS

The experimental campaigns were part of two research projects. The type ATCC-A has been conducted within the project "Adhesively bonded timber-concrete composites – pilot tests on the suitability of a commercially available epoxy resin adhesive" between the University of Kassel and fischerwerke GmbH & Co. KG, Germany. The type ATCC-B has been conducted within the project "Development of a rapid construction method for ATCC floors by means of bonding prefabricated concrete components" between the University of Kassel and BEWO-Betonfertigteile GmbH, Germany. The latter project is supported by the German Federal Ministry of Economics and Technology under the reference code ZF4147005EB9.

The authors would like to thank the research associations which funded and supervised the projects. Moreover, thanks goes to the associated companies Lübbert Warenhandel GmbH und Co. KG, Gebr. Schütt KG and RAMPF Machine Systems GmbH & Co. KG for their support and provision of materials.

REFERENCES

[1] Schmidt-Thrö G., Scheufer W., Fischer O.: Kontinuierliche faseroptische Dehnungsmessung im Stahlbetonbau, *Beton Stahlbetonbau* 111:496–504, 2016. https://doi.org/10. 1002/best.201600026

[2] Lemcherreq Y., Kaufmann W., Vogel T.: Fatigue of bond: Experimental investigation using pull-out tests with distributed fibre optical sensors. fib Symposium: Concrete Structures for Resilient Society (virtual) 2020.

[3] Könke C., Kuhne M., Beinersdorf H., Hildebrand J., Ganß M.: Monitoring von Klebverbindungen mittels faseroptischen Messsystem, Bauhaus-Universität Weimar and MPA Weimar, Report IGF: 17777 BR, 2015.

[4] Spangenberg A.-C.: Testing the use of fibre-optic measurement technology for monitoring bonded timber-concrete composite structures (Erprobung des Einsatzes faseroptischer Messtechnik für das Monitoring geklebter Holz-Beton-Verbundtragwerke), master thesis, 2022.

[5] Claus T., Seim W., Küllmer J.: Force distribution in self-tapping screws: experimental investigations with fibre Bragg grating measurement screws. *European Journal of Wood and Wood Products* 80:183–197, 2022. https://doi.org/10.1007/s00107-021-01740-z

[6] Frohnmüller J., Fischer J., Seim W.: Full-scale testing of adhesively bonded timber-concrete composite beams. *Materials and Structures* 54(5):1–21, 2021. Doi: https://doi.org/10.1617/s11527-021-01766-y

[7] Frohnmüller J., Seim W., Hummel J., Umbach C.: Adhesively bonded Timber-Concrete-Composite construction method (ATCC) – pilot application in a school building in Germany. WCTE 2023. Oslo, Norway, 2023.

[8] Galkovski T., Lemcherreq Y., Mata-Falcón J., Kaufmann W.: Fundamental Studies on the Use of Distributed Fibre Optical Sensing on Concrete and Reinforcing Bars. *Sensors* 21: 7643, 2021. https://doi.org/10.3390/s21227643